Climate sensitivity from both physical and carbon cycle feedbacks

Philip Goodwin[1], Richard G. Williams[2], Vassil Roussenov[2] and Anna Katavouta[2]

Author Accepted Manuscript

Accepted for publication in Geophysical Research Letters (13th June 2019)

This version submitted 6th June 2019

[1]Ocean and Earth Science, National Oceanography Centre Southampton, University of Southampton, Southampton, UK.

[2]Department of Earth, Ocean & Ecological Sciences, School of Environmental Sciences, University of Liverpool, Liverpool, UK.

ORCID ID P. Goodwin: 0000-0002-2575-8948
ORCID ID R.G. Williams: 0000-0002-3180-7558
ORCID ID V. Roussenov: 0000-0003-4128-9712
ORCID ID A. Katavouta: 0000-0002-1587-4996

Abstract

The surface warming response to anthropogenic forcing is highly sensitive to the strength of feedbacks in both the physical climate and carbon-cycle systems. However, the definitions of climate feedback, $\lambda_{\mathrm{Climate}}$ in Wm^{-2}K^{-1}, and climate sensitivity, S_{Climate} in K[Wm^{-2}]$^{-1}$, explicitly exclude the impact of carbon-cycle feedbacks. Here, we provide a new framework to incorporate carbon feedback into the definitions of climate feedback and sensitivity. Applying our framework to the Global Carbon Budget reconstructions reveals a present-day terrestrial carbon feedback of $\lambda_{\mathrm{Carbon}}$=0.31±0.09 Wm^{-2}K^{-1} and an ocean carbon feedback of -0.06 to 0.015 Wm^{-2}K^{-1} in Earth system models. Observational constraints reveal a combined climate and carbon feedback of $\lambda_{\mathrm{Climate+Carbon}}$=1.48 Wm^{-2}K^{-1} with a 95% range of 0.76 to 2.32 Wm^{-2}K^{-1} on centennial timescales, corresponding to a combined climate and carbon sensitivity of $S_{\mathrm{Climate+Carbon}}$=0.67 K[Wm^{-2}]$^{-1}$ with a 95% range of 0.43 to 1.32 K[Wm^{-2}]$^{-1}$.

Plain Language Summary

Feedback processes in the physical climate system and the carbon cycle affect the Earth's climate response to emissions of greenhouse gases, such as carbon dioxide. Physical climate feedbacks include the responses of clouds and atmospheric water vapor to rising surface temperatures, while carbon cycle feedbacks affect how much of the emitted carbon dioxide is removed from the atmosphere and stored in the ocean and on land. Conventionally, definitions of climate feedback and climate sensitivity include all the feedbacks in the physical climate system, but do not include carbon cycle feedbacks. This study provides a new framework to incorporate carbon feedback into the definitions of climate feedback and sensitivity. Evaluating the historical strengths of physical climate system and carbon cycle feedbacks suggests emissions of carbon dioxide will cause equilibrium (century timescale) surface warming to increase by between 0.6 to 2.0 °C for every 1000 PgC emitted when an equilibrium is approached between the atmosphere and ocean over many centuries.

1. Introduction

Climate change is driven by a combination of radiative forcing and climate feedbacks operating in the climate system (see review in *Knutti et al*., 2017). The climate feedback is usually expressed in terms of the change in surface temperature multiplied by a feedback parameter, λ in $Wm^{-2}K^{-1}$, defined in terms of a wide range of physical processes, including the Planck response of enhanced longwave emission from a warmer surface and physical feedbacks from changes in water vapour, lapse rate, cloud cover and ice albedo (*Gregory et al.,* 2004*; Andrews et al.,* 2012*, Armour et al.,* 2013*; Andrews et al.,* 2015*; Ceppi and Gregory*, 2017). In contrast, the carbon-cycle responses and feedbacks are usually defined in terms of how atmospheric carbon dioxide and temperature linearly combine to alter the carbon inventories of the climate system (*Friedlingstein et al*., 2003, 2006; *Arora et al*., 2013), which may be expressed in terms of a radiative feedback parameter in $Wm^{-2}K^{-1}$ (*Gregory et al*., 2009). However, there are difficulties in applying this carbon feedback method due to nonlinearities in how the separate atmospheric carbon dioxide and temperature effects combine together (*Schwinger et al*., 2014) giving rise to errors in the overall carbon feedback (*Arora et al*., 2013). This linearization method also cannot be used to calculate the carbon feedback directly from observational reconstructions of the carbon cycle (e.g. *le Quéré et al*., 2018), since there is no observational method to generate the hypothetical state with a range of feedback processes turned off for the real world.

The separation of forcing and feedback is dependent upon the nature of the climate perturbation. In climate model experiments driven by an imposed atmospheric CO_2 trajectory, a radiative forcing is provided from the increase in atmospheric CO_2 that automatically includes the effects of carbon-cycle feedbacks. In contrast, for climate model experiments driven by carbon emissions, a radiative forcing is provided from the increase in atmospheric CO_2 directly caused by the carbon emission together with a radiative feedback from the change in atmospheric CO_2 caused by changes in the terrestrial and ocean carbon reservoirs.

To understand this distinction between forcing and feedback, consider the response of a conceptual Earth system model to a pulse of carbon released to the atmosphere, which is partitioned between the atmosphere, ocean and terrestrial systems (Fig. 1a). The original carbon release drives a radiative forcing from the increase in atmospheric CO_2 (Fig. 1b, red line), which is augmented by a radiative feedback from both non-CO_2 and CO_2 changes (Fig. 1c, yellow and blue lines). These feedbacks may act to enhance or oppose the original forcing perturbation.

Our aim is to define and evaluate a new feedback parameter for the carbon system that:

(1) Takes into account the combined effects of the non-CO_2 and CO_2 feedbacks operating in the climate system, thus avoiding the need to make a linearizing assumption that introduces error;

(2) Allows direct comparison between magnitudes of, and uncertainties in, feedbacks in the climate and carbon systems; and

(3) Allows the practical application of real-world observational data to analyze carbon feedback.

2. Definition of a climate and carbon feedback parameter

Consider the global energy balance for a climate system perturbed from an initial steady state (e.g. Fig. 1a,b). The radiative forcing perturbation, $\Delta R'$, from the original forcing perturbation combined with subsequent feedback terms is balanced by additional outgoing longwave radiation emitted due to surface warming, $\lambda_{\mathrm{Planck}}\Delta T$, and the net Earth system heat uptake, *N,* all terms defined in Wm^{-2},

$$\Delta R' = \lambda_{Planck}\Delta T + N, \tag{1}$$

where $\lambda_{\mathrm{Planck}}$ is the Planck feedback parameter in $\mathrm{Wm}^{-2}\mathrm{K}^{-1}$ and ΔT is the change in global-mean surface temperature in K. The radiative forcing, $\Delta R'$, consists of an original forcing perturbation, $\Delta R^{forcing}$ plus a subsequent feedback term, $\Delta R^{feedback}$, $\Delta R' = \Delta R^{forcing} + \Delta R^{feedback}$, and the feedback may be written in terms of the separate non-CO_2 and CO_2 components, $\Delta R^{feedback}_{non-CO2}$ and $\Delta R^{feedback}_{CO2}$ respectively (Fig. 1b), such that

$$\Delta R' = \Delta R^{forcing} + \Delta R^{feedback}_{non-CO2} + \Delta R^{feedback}_{CO2}\ . \tag{2}$$

The radiative feedback term from non-CO_2 feedbacks, $\Delta R^{feedback}_{non-CO2}$, includes the effects of changes in water vapor, lapse rate, clouds and surface albedo, while the radiative feedback term from CO_2, $\Delta R^{feedback}_{CO2}$, includes how radiative forcing from atmospheric CO_2 is altered by changes in the ocean and terrestrial carbon inventories.

The radiative response is often defined in terms of a climate feedback, $\lambda_{Climate}\Delta T$ in Wm^{-2}, by combining the Planck response, $\lambda_{Planck}\Delta T$, with the radiative forcing from non-CO_2 feedbacks, $\Delta R^{feedback}_{non-CO2}$ (e.g. see IPCC, 2013; *Knutti et al.*, 2017),

$$\lambda_{Climate}\Delta T = \lambda_{Planck}\Delta T - \Delta R^{feedback}_{non-CO2}, \tag{3}$$

such that the energy balance in (1) may be re-expressed from (2) and (3) by

$$\Delta R^{forcing} + \Delta R_{CO2}^{feedback} = \lambda_{Planck}\Delta T - \Delta R_{non-CO2}^{feedback} + N = \lambda_{Climate}\Delta T + N \, . \quad (4)$$

The standard form of the climate feedback definition in (3) does not encapsulate the full sensitivity of the Earth system to perturbation, as the definition only accounts for the strength of the non-CO_2 feedbacks in the system and ignores the impact of carbon-cycle feedbacks, which are instead treated as part of the forcing perturbation in (4). Here, we re-express the energy-balance relations (1) and (4) using a new combined carbon plus climate feedback, $\lambda_{\mathrm{Climate+Carbon}}$ in $Wm^{-2}K^{-1}$, defined as the sum of the climate and carbon feedbacks,

$$\lambda_{Climate+Carbon}\Delta T = \lambda_{Planck}\Delta T - \Delta R_{non-CO2}^{feedback} - \Delta R_{CO2}^{feedback} = (\lambda_{Climate} + \lambda_{Carbon})\Delta T, \quad (5)$$

where $\lambda_{Carbon} = -\,\Delta R_{CO2}^{feedback}/\Delta T$. The energy balance in (1) may now be more explicitly written in terms of the original radiative forcing, $\Delta R^{forcing}$, balancing the radiative response from the combined climate and carbon responses, $\lambda_{Climate+Carbon}\Delta T$, plus the planetary heat uptake, N, such that

$$\Delta R^{forcing} = \lambda_{Climate}\Delta T - \Delta R_{CO2}^{feedback} + N = \lambda_{Climate+Carbon}\Delta T + N. \quad (6)$$

To progress, we now wish to evaluate the carbon feedback λ_{Carbon} in terms of changes in ocean and terrestrial carbon inventories.

3. Extracting the feedback component to CO_2 change

A small carbon emission into a preindustrial state, δI_{em} in PgC, is distributed between the atmospheric, ocean and terrestrial carbon reservoirs (Fig. 1a),

$$\delta I_{em} = \delta I_{atmos} + \delta I_{ocean} + \delta I_{ter} = M\delta \mathrm{CO}_2 + V\delta C_{DIC} + \delta I_{ter}, \quad (7)$$

where $\delta I_{atmos}=M\delta CO_2$ is the change in atmospheric CO_2 inventory since the preindustrial, with M the molar volume of the atmosphere and CO_2 the atmospheric CO_2 mixing ratio; $\delta I_{ocean}=V\delta C_{DIC}$ is the change in ocean dissolved inorganic carbon (DIC) inventory, with V the ocean volume and C_{DIC} the mean-ocean concentration of DIC; δI_{ter} is the change in terrestrial (soil + vegetation) carbon inventory; and the symbol δ is used to indicate a small infinitesimal change since the preindustrial.

Radiative forcing is related to the log change in atmospheric CO_2, $R_{CO2} = a\Delta \ln \mathrm{CO_2}$ (*Myhre et al*, 2013), so that our goal is to find an expression for the change in log CO_2 due to some initial carbon emission, δI_{em}, and subsequent responses to forcing and feedbacks within the atmosphere-ocean-terrestrial carbon system (7). The ocean inventory of carbon involves the dissolved inorganic carbon concentration C_{DIC}, which may be expressed as a sum of process-driven components (*Ito and Follows*, 2005; *Goodwin et al.*, 2008, *Williams and Follows,* 2011) involving the DIC concentration at chemical saturation with atmospheric CO_2, C_{sat}, the disequilibrium concentration at subduction, C_{dis}, and the DIC contribution from regenerated biological material, C_{bio}, (C_{DIC}=C_{sat}+C_{dis}+C_{bio}: Appendix). Applying this ocean partitioning allows the perturbation to the global carbon inventory (7) to be re-expressed as

$$\delta I_{em} = \left(I_{atmos} + \frac{VC_{sat}}{B}\right)\delta \ln \mathrm{CO_2} + V\left(\delta C_{dis} + \delta C_{bio} + \frac{\partial C_{sat}}{\partial A_{pre}}\delta A_{pre} + \frac{\partial C_{sat}}{\partial T_{oc}}\delta T_{oc}\right) + \delta I_{ter}, \qquad (8)$$

where A_{pre} is the global mean ocean preformed titration alkalinity; T_{oc} is the global mean ocean temperature; B=$\partial \ln CO_2/\partial \ln C_{sat}$ is the Revelle Buffer factor of seawater; and $I_{atmos} + (VC_{sat}/B) = I_B$ is the buffered carbon inventory of the air-sea system (*Goodwin et al.*, 2007; 2008; 2015).

Re-arranging (8) for $\delta \ln CO_2$, and integrating for large changes using a constant buffered carbon inventory approximation (*Goodwin et al.*, 2007; 2008; 2009; 2011; 2015: Appendix), decomposes ΔR_{CO2} into the initial response to forcing from anthropogenic carbon emissions in the absence of feedbacks, $\Delta R_{CO2}^{forcing}$, plus components from terrestrial and ocean carbon cycle feedbacks, $\Delta R_{CO2}^{feedback} = \Delta R_{terrestrial}^{feedback} + \Delta R_{ocean}^{feedback}$ (Fig. 1a,b), such that

$$\Delta R_{CO2} = \Delta R_{CO2}^{forcing} + \Delta R_{CO2}^{feedback} = \Delta R_{CO2}^{forcing} + \Delta R_{terrestrial}^{feedback} + \Delta R_{ocean}^{feedback}, \qquad (9)$$

where $\Delta R_{CO2}^{forcing}$ is related to terms involving the carbon emission ΔI_{em} and the change in ocean disequilibrium carbon ΔC_{dis} from (8); $\Delta R_{terrestrial}^{feedback}$ is related to the feedback from the change in the terrestrial carbon inventory, ΔI_{ter}; and $\Delta R_{ocean}^{feedback}$ is related to the feedback from the changes in the ocean carbon inventory involving the saturated and regenerated carbon pools (8) from ΔC_{bio}, ΔA_{pre} and ΔT_{oc} (Appendix).

4. Evaluating carbon feedback from observational constraints and numerical simulations

4.1 Terrestrial carbon feedback

The change in the radiative forcing, $\Delta R_{terrestrial}^{feedback}$ in (9), is related to the change in the cumulative terrestrial carbon inventory relative to the preindustrial, ΔI_{ter} in PgC (Fig. 1a,b; *Goodwin et al.*, 2007: 2008; 2009; 2011; 2015: Appendix), which is given by

$$\Delta R_{terrestrial}^{feedback} = -\left(\frac{a}{I_B}\right)\Delta I_{ter}. \qquad (10)$$

The terrestrial carbon feedback λ_{Carbon} is diagnosed from reconstructions of the change in the terrestrial carbon inventory and surface temperature record by substituting (10) into (5),

$$\lambda_{Carbon} = -\frac{\Delta R_{terrestrial}^{feedback}}{\Delta T} = -\left(\frac{a}{I_B}\right)\frac{\Delta I_{ter}}{\Delta T} \qquad (11)$$

This new relation (11) is now used to quantify terrestrial carbon feedback from observational reconstructions and Earth system model simulations. λ_{Carbon} is estimated using the following parameters: the radiative forcing coefficient from CO_2, a=5.35±0.27 Wm^{-2} (*Myhre et al.*, 2013); the buffered carbon inventory, I_B=3451±96 PgC (*Williams et al.*, 2017); the global-mean surface temperature change ΔT is from the GISTEMP temperature record (*Hansen et al*. 2010), including an 11-average smoothing (Fig. 2a, black dotted and full lines); and change in the terrestrial carbon inventory ΔI_{ter} are from the Global Carbon Budget (*le Quéré et al*., 2018) (Fig. 2b, black). Uncertainties in the terrestrial carbon budget are taken from the additional data for the 16 individual dynamic global vegetation models (DGVMs) in the Global Carbon Budget (*le Quéré et al*., 2018; Supplementary Information; Acknowledgements).

These historical reconstructions for the terrestrial carbon inventory and surface temperature reveal an observation-constrained estimate of the terrestrial carbon feedback parameter, $\lambda_{\mathrm{Carbon}}=0.33\pm0.09$ $\mathrm{Wm^{-2}K^{-1}}$ for the present day (Fig. 2c, black line and shading), which represents a negative feedback that reduces global warming through terrestrial carbon uptake. The strength of this negative feedback reached a peak magnitude of $\lambda_{\mathrm{Carbon}} = 0.86\pm0.34$ $\mathrm{Wm^{-2}K^{-1}}$ in the late 1960s, but then has decreased in time as the rate of increase in surface warming since the early 1970s (Fig. 2a, black) (*Hansen et al*., 2010) has not matched the rate of increase in the cumulative terrestrial carbon sink (Fig. 2b, black) (*le Quéré et al*., 2018).

The terrestrial carbon feedback is now evaluated from four CMIP5 Earth system models (CanESM2, HadGEM2-ES, HadGEM2-CC and NorESM-ME), chosen as these have a reliable net export production (nep) variable allowing calculation of ΔI_{ter} in (11). From the simulated ΔI_{ter} and 11-year average ΔT (Fig. 2a,b), and estimates of a and I_B for each model (*Williams et al*. 2017), $\lambda_{\mathrm{Carbon}}$ is evaluated from year 1959 to 2100 for the RCP4.5 scenario (Fig. 2c). These four CMIP5 Earth system models have a smaller present-day terrestrial carbon feedback parameter ranging from 0.02 to 0.65 $\mathrm{Wm^{-2}K^{-1}}$, broader than the 1σ range from observational reconstructions (Fig. 2c, compare dashed lines to black line and shading). These differences between the Earth system models and the observational estimate arise from their discrepancy between the modeled and observational reconstructions of surface warming and terrestrial carbon uptake (Fig. 2a,b). The future simulated $\lambda_{\mathrm{Carbon}}$ remains stable under the RCP4.5 scenario, remaining close to the present-day values to year 2100 (Fig 2c).

Additional projections of carbon feedback are made using a very large ensemble of observation-constrained simulations from the Warming Acidification and Sea level Projector (WASP: *Goodwin*, 2016), for the RCP4.5 scenario (Fig. 2, blue line and shading). We adopt the WASP model configuration of *Goodwin* (2018), with climate feedback including components from different processes operating on different response timescales (Fig. 1). An ensemble is generated of many thousands of observation-consistent simulations using the Monte Carlo plus history matching (*Williamson et al*., 2015) methodology of *Goodwin et al*. (2018). First, the initial ensemble of 10-million Monte Carlo simulations is generated as in *Goodwin* (2018), with varied model input parameters, and integrate each simulation from years 1765 to 2017 with historical forcing. Next the observational-consistency test of *Goodwin* (2018 – see Table 2 therein) is applied with an updated terrestrial carbon range (Supplementary Table S1) based on the 16 observation-consistent DGVMs of the Global Carbon Budget 2018 (*le Quéré et al*. 2018). Only 6273 simulations pass the observation-consistency test and a further 3 simulations are rejected as non-physical since $\lambda_{\mathrm{Climate}}$ becomes negative on long timescales.

The remaining ensemble of 6270 WASP simulations are then consistent with historic observations of surface warming (Fig. 2a, compare blue to black), terrestrial carbon uptake (Fig. 2b, compare blue to black) and ocean heat content changes (Supplementary Table S1; Goodwin, 2018). Due to the observation-simulation agreement in ΔT and ΔI_{ter}, the final WASP ensemble is also in good agreement with the observational reconstructions of terrestrial $\lambda_{\mathrm{Carbon}}$ using (11) from years 1959 to 2017 (Fig. 2c, compare blue to black). Under the RCP4.5 scenario, the observation-constrained WASP ensemble shows a similar future behavior as in the response of the CMIP5 models (Fig. 2c, compare blue solid line and shading to dashed lines), with $\lambda_{\mathrm{Carbon}}$ displaying only a small change in magnitude from the present day towards year 2100.

4.2 Ocean carbon feedback

In a similar manner to how the terrestrial carbon feedback is defined relative to ΔI_{ter} (11), the ocean carbon feedback is defined in relation to changes in the ocean DIC from regenerated carbon, $\Delta C_{bio},$ and changes in the ocean saturated carbon inventory from preformed alkalinity ΔA_{pre} and ocean temperature ΔT_{oc} (eqns. 8, A8), via,

$$\lambda_{Carbon} = -\frac{\Delta R_{ocean}^{feedback}}{\Delta T} = -\left(\frac{a}{I_B}\right)\frac{\Delta C_{bio} + \left(\partial C_{sat}/\partial A_{pre}\right)\Delta A_{pre} + \left(\partial C_{sat}/\partial T_{oc}\right)\Delta T_{oc}}{\Delta T}. \tag{12}$$

This ocean feedback term represents how changes in ocean temperature and ocean biological cycling of carbon and alkalinity from an initial carbon perturbation then feedback to alter the radiative forcing from atmospheric CO_2. Based on Earth system models (evaluating ΔC_{bio}, ΔA_{pre} and ΔT_{oc}), observational reconstructions for ocean heat uptake (*Cheng et al*., 2017) and the WASP ensemble (both evaluating ΔT_{oc} only), the ocean carbon feedback is diagnosed as being much smaller than the terrestrial carbon feedback in the present day, ranging from -0.015 to 0.06 $\mathrm{Wm^{-2}K^{-1}}$ (Fig. 2c,d), and remains small for the 21st century. The magnitude of the ocean carbon feedback might though increase beyond year 2100 due to continued climate-driven changes in ocean temperature, ΔT_{oc}, and ocean biological carbon drawdown, ΔC_{bio}.

Our estimate of ocean carbon feedback (Fig. 2d) is much smaller than that implied by *Gregory et al*. (2009) because the previous approach (*Friedlingstein et al*., 2006) considers the transient disequilibrium of ocean DIC, C_{dis} (eq. 8), to be part of the ocean carbon feedback, while our method considers C_{dis} as part of the transient ocean response. An idealized feedback grows in magnitude over time, from zero the instant a forcing is applied to some final equilibrium value on long timescales. We do not consider C_{dis} part of the ocean carbon feedback because the time-evolution of C_{dis} is the opposite sense: ocean CO_2 disequilibrium is large the instant CO_2 is emitted into the atmosphere and then decays to zero over long timescales due to ocean carbon uptake (Supplementary Fig. S1).

5. Estimating the combined carbon-climate feedback and sensitivity

We now place observational constraints on the combined climate plus carbon feedback, $\lambda_{\text{Climate+Carbon}}$, and sensitivity, $S_{\text{Climate+Carbon}}$ in K[Wm^{-2}]$^{-1}$, by evaluating both λ_{Climate} and λ_{Carbon} for an idealized perturbation experiment in the observation constrained WASP ensemble. Each of the 6270 observation-consistent WASP ensemble members (Fig. 2, blue line and shading) is reinitialized at a preindustrial spin up and integrated for 500 years, forced with an idealized scenario consisting of a 1000 PgC emission over the first 100 years (Fig. 1a).

The total radiative forcing $\Delta R'$ is decomposed into the initial emission forcing, $\Delta R_{CO2}^{forcing}$, non-CO_2 feedback, $\Delta R_{non-CO2}^{feedback}$, and CO_2 feedback, $\Delta R_{CO2}^{feedback}$, terms (Fig. 1b) using eqns. (1)-(6). From this decomposition, $\lambda_{Climate}$ and λ_{Carbon} (Figs. 1c,d) are evaluated over multiple response timescales in the observation-consistent ensemble, where the λ_{Climate} results are comparable to the similarly constrained ensemble in *Goodwin* (2018 – see figure 2 therein). Here, λ_{Carbon} in WASP includes both the larger terrestrial and smaller ocean temperature-CO_2 solubility effects (Fig. 1d), but WASP does not simulate changes in C_{bio}, which remain small in Earth system models (Fig. 2d). For illustration purposes, $\lambda_{Climate}$ and λ_{Carbon} contributions from individual processes are shown by integrating the WASP ensemble with combinations of feedback processes switched off (Fig. 1c,d, dashed lines are ensemble median values).

Estimates of the carbon and climate feedback parameters, λ_{Carbon} and λ_{Climate}, applicable on century timescales, are made from the observation-consistent ensemble distributions at the end of the 1000PgC emission simulations (Fig. 1). The 500-year carbon feedback after a 1000PgC emission has a median (and 95% range) of λ_{Carbon} = 0.21 (-0.02 to 0.5) Wm^{-2}K^{-1} (Fig. 1c), while the physical climate feedback after a 1000PgC emission is λ_{Climate}=1.27 (0.73 to 1.88) Wm^{-2}K^{-1} (Fig. 1b, Fig 3a, blue).

The impact of carbon feedbacks is therefore to increase the overall carbon plus climate feedback above λ_{Climate}, with an observation-constrained distribution of $\lambda_{\text{Climate+Carbon}}=\lambda_{\text{Carbon}}+\lambda_{\text{Climate}}=1.48$ (0.76 to 2.32) $Wm^{-2}K^{-1}$ (Fig. 3a). Consequently, the climate sensitivity, $S=1/\lambda$, from non-CO_2 feedbacks alone, S_{Climate}= 0.79 (0.53 to 1.37) $K[Wm^{-2}]^{-1}$, is reduced to $S_{\text{Climate+Carbon}}$=0.67 (0.43 to 1.32) $K[Wm^{-2}]^{-1}$, when encapsulating both non-CO_2 and CO_2 feedbacks acting together (Fig. 3b). This estimate of $S_{\text{Climate+Carbon}}$ (Fig. 3b, black) represents the total sensitivity of the climate system to perturbation by carbon emission over century timescales, including both physical climate and carbon-cycle feedbacks.

6. Conclusions

A new method is presented to constrain the carbon feedback parameter, finding for the present-day terrestrial carbon system $\lambda_{\text{Carbon}}=0.33\pm0.09 Wm^{-2}K^{-1}$ (Fig. 2c) based on observational reconstructions of carbon uptake and warming (*le Quéré et al*. 2018; *Hansen et al*., 2010), and λ_{Carbon}=0.02 to 0.65 $Wm^{-2}K^{-1}$ in four CMIP5 models. This compares to a previous method implying terrestrial carbon feedback of $\lambda_{\text{Carbon}}=0.7\pm0.5$ $Wm^{-2}K^{-1}$, based on analysis of the earlier C4MIP climate model ensemble (*Arneth et al*., 2010; *Gregory et al*., 2009; *Friedlingstein et al*., 2006) and comprising a linearization of separate CO_2-carbon ($1.1\pm0.5 Wm^{-2}K^{-1}$) and climate-carbon ($-0.4\pm0.2 Wm^{-2}K^{-1}$) components. The linearization assumed by the previous method introduces errors (*Schwinger et al*. 2014; *Arora et al*., 2013) and means the method cannot be applied to observational reconstructions. To avoid making the linearization assumption, and so be applicable to observational reconstructions, our method assumes a constant buffered carbon inventory (Appendix); a good approximation for carbon perturbations up to ~5000PgC or for atmospheric CO_2 reaching ~1100ppm (*Goodwin et al*., 2007; 2008; 2009).

The Equilibrium Climate Response to Emission, ECRE in K $1000PgC^{-1}$, expresses the warming per unit carbon emitted once ocean heat uptake approaches zero over centennial to multi-centennial timescales, ECRE=$\Delta T/\Delta I_{em}$ (Frölicher & Paynter 2015). This atmosphere-ocean equilibrium is approached over many centuries, but not necessarily reached due to the effect of other longer timescale carbon and climate feedbacks, such as from ice sheet-albedo feedbacks (Rohling et al., 2018) and multi-millennial $CaCO_3$ sediment and weathering responses (Archer et al., 2005). In the absence of carbon feedbacks, *Williams et al*. (2012) related the ECRE to climate feedback, $\lambda_{Climate}$, via $\text{ECRE} = a/(\lambda_{climate} I_B)$. Here, we extend the relationship to include the effects of both climate and carbon feedbacks, $\text{ECRE} = a/(\lambda_{climate+carbon} I_B)$, applicable after ocean CO_2 invasion and heat uptake but prior to significant $CaCO_3$ sediment and weathering responses (Archer, 2005; Goodwin et al., 2007; 2008; 2015). Our historically constrained feedback estimates (Fig. 3a,b) imply ECRE =1.0 (0.6 to 2.0) K per 1000PgC emitted (Fig. 3c), with the upper half of our range (from 1 to 2 K$[1000\text{PgC}]^{-1}$) consistent with a CMIP5-based estimate (Frölicher & Paynter, 2015). Carbon and climate feedbacks not constrained historically (e.g. Rohling et al., 2018; Zickfield et al., 2013; Pugh et al., 2018; MacDougall & Knutti, 2016), may alter future $\lambda_{climate+carbon}$ and so alter ECRE. We anticipate this relationship, ECRE $= a/(\lambda_{climate+carbon} I_B)$, will be useful in elucidating how different carbon and climate feedbacks contribute to the multi-century warming response to carbon emission.

Appendix: Connecting radiative feedbacks to changes in carbon inventories

Our aim is to separate the total CO_2 radiative forcing into a sum of linearly-separable terms representing different processes and feedbacks. We start by considering how carbon emissions perturb carbon storage across the atmosphere-ocean-terrestrial system. We now write identities for the changes in atmospheric and ocean carbon inventories containing terms with δlnCO2. Using the identity for small perturbations in x, $\delta x = x \delta \ln x$, we write an identity for a small perturbation in atmospheric CO_2 inventory, δI_{atmos}, in terms of a small perturbation to the logarithm of atmospheric CO_2, $\delta \ln CO_2$,

$$\delta I_{atmos} = I_{atmos} \delta \ln \mathrm{CO_2}, \qquad \text{(A1)}$$

where I_{atmos} is the initial atmospheric CO_2 inventory at the unperturbed preindustrial state.

The change in ocean DIC is considered, via a process-driven viewpoint (*Ito and Follows*, 2005; *Goodwin et al*., 2008; *Williams and Follows*, 2011), in terms of the sum of components from the change in chemically-saturated DIC arising from changes in atmospheric CO_2 and seawater properties, δC_{sat}, the change in chemical disequilibrium of ocean DIC relative to atmospheric CO_2, δC_{dis}, and the combined change in ocean DIC from regenerated soft tissue and $CaCO_3$ drawdown, δC_{bio},

$$\delta C_{DIC} = \delta C_{sat} + \delta C_{dis} + \delta C_{bio}. \qquad \text{(A2)}$$

Due to the carbonate chemistry system, the perturbation to C_{sat} is a function of the change to the logarithm of atmospheric CO_2, $\delta \ln CO_2$, the change in mean ocean preformed titration alkalinity, δA_{pre}, the change in mean seawater temperature, δT_{oc}, and the change in mean seawater salinity, δS: $\delta C_{sat} = \delta C_{sat}(\delta \ln \mathrm{CO}_2, \delta A_{pre}, \delta T_{oc}, \delta S)$. This small perturbation to C_{sat} is now expanded after *Goodwin and Lenton* (2009) into components from $\delta \ln CO_2$, δA_{pre}, δT_{oc}, and δS,

$$\delta C_{dis} = \frac{\partial C_{sat}}{\partial \ln \mathrm{CO}_2} \delta \ln \mathrm{CO}_2 + \frac{\partial C_{sat}}{\partial A_{pre}} \delta A_{pre} + \frac{\partial C_{sat}}{\partial T_{oc}} \delta T_{oc} + \frac{\partial C_{sat}}{\partial S} \delta S, \qquad \text{(A3)}$$

where the salinity term, $(\partial C_{sat}/\partial S)\delta S$, is small and henceforth will be omitted.

Again, using the identity for small perturbations in a variable x, $\delta x = x\delta \ln x$, but applying to C_{sat}, the term for the sensitivity of C_{sat} to $\ln CO_2$ in (A3) becomes,

$$\frac{\partial C_{sat}}{\partial \ln \mathrm{CO}_2} \delta \ln \mathrm{CO}_2 = C_{sat} \frac{\partial \ln C_{sat}}{\partial \ln \mathrm{CO}_2} \delta \ln \mathrm{CO}_2 = \frac{C_{sat}}{B} \delta \ln \mathrm{CO}_2, \qquad \text{(A4)}$$

where $B=(\partial \ln CO_2/\partial \ln C_{sat})$ is the Revelle Buffer factor expressing how fractional chemical in atmospheric CO_2 are much larger than fractional changes in DIC with B the order 10 for the present ocean (e.g. *Williams and Follows*, 2011). Substituting (A4) into (A3), and noting that $I_{ocean}=VC_{DIC}$, produces an identity for δI_{ocean} containing a term in $\delta \ln CO_2$,

$$\delta I_{ocean} = \frac{I_{ocean}^{sat}}{B} \delta \ln \mathrm{CO}_2 + V\left(\delta C_{dis} + \delta C_{bio} + \frac{\partial C_{sat}}{\partial A_{pre}} \delta A_{pre} + \frac{\partial C_{sat}}{\partial T_{oc}} \delta T_{oc}\right), \qquad \text{(A5)}$$

where $I_{ocean}^{sat} = VC_{sat}$ is the ocean inventory of saturated DIC at current atmospheric CO_2 . Substituting δI_{ocean} (A5) and δI_{atmos} (A1) into (7), and re-arranging to solve for the log change in atmospheric CO_2 mixing ratio to small perturbations to I_{em}, I_{ter}, C_{dis}, C_{bio}, A_{pre} and T_{oc}, reveals

$$\left(I_{atmos} + \frac{I_{ocean}^{sat}}{B}\right) \delta \ln \mathrm{CO}_2 = \delta I_{em} - \delta I_{ter} - V\left(\delta C_{dis} + \delta C_{bio} + \frac{\partial C_{sat}}{\partial A_{pre}} \delta A_{pre} + \frac{\partial C_{sat}}{\partial T_{oc}} \delta T_{oc}\right)$$

(A6)

The issue now is that this identity for $\delta \ln CO_2$, (A7), applies only to small infinitesimal perturbations, and we wish to solve for the change in log CO_2 for large finite perturbations. The next step is therefore to integrate (A6) over large finite perturbations in I_{em}, I_{ter}, C_{dis}, C_{bio}, A_{pre} and T_{oc}.

To integrate (A6), we note that the left-hand side contains the buffered carbon inventory, I_B (*Goodwin et al.*, 2007; 2008), defined as the atmospheric carbon inventory added to the ocean saturated-DIC inventory divided by the Revelle Buffer factor, $I_B = I_{atmos} + \left(I_{ocean}^{sat}/B\right)$. I_B represents the total buffered CO_2 and DIC in the atmosphere-ocean system that is available for redistribution between the CO_2 and carbonate ion pools (*Goodwin et al.*, 2009), given that the majority of ocean DIC is in the form of bicarbonate ions. At the preindustrial state, I_B=3451±96 PgC in the CMIP5 models analyzed by *Williams et al*. (2017).

Using this constant buffered carbon inventory approach (Supplementary), we integrate (A6) to find the change in atmospheric CO_2 for large finite perturbations to total carbon emitted, ΔI_{em}, the change in terrestrial carbon storage, ΔI_{ter}, the large changes in mean ocean values of ΔC_{dis}, ΔC_{bio}, ΔA_{pre} and ΔT_{oc}, so that

$$I_B \Delta \ln \mathrm{CO_2} = \Delta I_{em} - \Delta I_{ter} - V\left(\Delta C_{dis} + \Delta C_{bio} + \frac{\partial C_{sat}}{\partial A_{pre}}\Delta A_{pre} + \frac{\partial C_{sat}}{\partial T_{oc}}\Delta T_{oc}\right). \quad \text{(A7)}$$

Multiplying (A7) by the CO_2-radiative forcing coefficient, a, produces an expression for the radiative forcing from CO_2 in (9),

$$\Delta R_{CO2} = \Delta R_{CO2}^{forcing} + \Delta R_{terrestrial}^{feedback} + \Delta R_{ocean}^{feedback} \quad ,$$

as a sum of separable terms representing different processes, each linked to a different change in a carbon inventory. The CO_2 radiative forcing,

$$\Delta R_{CO2}^{forcing} = (a/I_B)(\Delta I_{em} - V\Delta C_{dis}), \quad \text{(A8a)}$$

represents the direct effect of the emitted carbon partitioned between the atmosphere and ocean, including both chemical equilibrium (ΔI_{em}) and the transient chemical disequilibrium between the atmosphere and ocean (ΔC_{dis}) of the carbon emitted, but without subsequent carbon feedbacks. The radiative forcing from the carbon feedbacks for the terrestrial,

$$\Delta R_{terrestrial}^{feedback} = -(a/I_B)\Delta I_{ter}, \quad \text{(A8b)}$$

depends on the change in terrestrial carbon storage since the preindustrial, and for the ocean

$$\Delta R_{ocean}^{feedback} == -(a/I_B)V\big(\Delta C_{bio} + \big[\partial C_{sat}/\partial A_{pre}\big]\Delta A_{pre} + [\partial C_{sat}/\partial T_{oc}]\Delta T_{oc}\big), \quad \text{(A8c)}$$

depends on the changes to the ocean biological drawdown of soft tissue and $CaCO_3$, including the titration alkalinity effects, and from changes in the seawater temperature since the preindustrial, altering the solubility of CO_2 in seawater.

Acknowledgements:
We acknowledge global surface temperature anomaly data from GISTEMP Team, 2018: GISS Surface Temperature Analysis (GISTEMP). NASA Goddard Institute for Space Studies. Dataset accessed 2018-01-16 at https://data.giss.nasa.gov/gistemp/. We acknowledge the Global Carbon Project's Global Carbon Budget 2018 for the land carbon sink data, including the multi-model mean from 16 DGVMs from year 1750 to 1959 and the model breakdowns from these models from years 1959 to 2017. We thank Stephen Sitch for providing additional data from these 16 Global Carbon Project DGVMs prior to 1959, allowing the inter-model standard deviation in the inter-model cumulative land carbon sink, ΔI_{ter}, to be calculated. The authors acknowledge the World Climate Research Programmes Working Group on Coupled Modelling responsible for CMIP5. This work was funded by UK NERC grant NE/N009789/1 and combined UK NERC/UK Government Department of BEIS grant NE/P01495X/1.

References:

Archer, D. (2005) Fate of fossil fuel CO2 in geologic time. *Journal of Geophysical Research*, 110 (C9), C09S05, doi:10.1029/2004JC002625.

Andrews, T., Gregory, J.M., Webb, M.J. and Taylor, K.E., (2012) Forcing, feedbacks and climate sensitivity in CMIP5 coupled atmosphere-ocean climate models. *Geophysical Research Letters*, *39*(9).

Andrews, T., Gregory, J.M. and Webb, M.J. (2015) The dependence of radiative forcing and feedback on evolving patterns of surface temperature change in climate models. *Journal of Climate*, *28*(4), pp.1630-1648.

Armour, K.C., Bitz, C.M. and Roe, G.H., (2013) Time-varying climate sensitivity from regional feedbacks. *Journal of Climate*, *26*(13), pp.4518-4534.

Arneth, A., Harrison, S.P., Zaehle, S., Tsigaridis, K., Menon, S., … & Vesala, T. (2010) Terrestrial biogeochemical feedbacks in the climate system, *Nature Geoscience* 3, 525-532.

Arora, V.K., Boer, G.J., Friedlingstein, P., Eby, M., Jones, C.D., Christian, J.R., Bonan, G., Bopp, L., Brovkin, V., Cadule, P. and Hajima, T. (2013) Carbon–concentration and carbon–climate feedbacks in CMIP5 Earth system models. *J. Climate*, *26*(15), pp.5289-5314.

Ceppi, P. and Gregory, J.M. (2017) Relationship of tropospheric stability to climate sensitivity and Earth's observed radiation budget. *Proceedings of the National Academy of Sciences*, *114*(50), pp.13126-13131.

Cheng, L. et al. (2017). Improved estimates of ocean heat content from 1960 to 2015. *Sci. Adv.* 3, e1601545.

Friedlingstein, P., Dufresne, J.L., Cox, P.M. and Rayner, P. (2003) How positive is the feedback between climate change and the carbon cycle?. *Tellus B*, *55*(2), pp.692-700.

Friedlingstein, P., Cox, P., Betts, R., Bopp, L., von Bloh, W., Brovkin, V., … and Bala, G., (2006) Climate–carbon cycle feedback analysis: results from the C4MIP model intercomparison. *J. Climate*, *19*(14), pp.3337-3353.

Frölicher, T. L. and Paynter, D.J. (2015) Extending the relationship between global warming and cumulative carbon emissions to multi-millennial timescales. *Environmental Research Letters*, 10 (7), 075 002.

Gillett, N.P., Arora, V.K., Matthews, D. and Allen, M.R., 2013. Constraining the ratio of global warming to cumulative CO_2 emissions using CMIP5 simulations. *J. Climate*, *26*(18), pp.6844-6858.

Goodwin, P., (2018) On the time evolution of climate sensitivity and future warming, *Earth's Future* 6, EFT2466, doi:10.1029/2018EF000889.

Goodwin. P., A. Katavouta, V.M. Roussenov, G.L. Foster, E.J. Rohling and R.G. Williams, (2018) Pathways to 1.5 and 2 °C warming based on observational and geological constraints, *Nature Geoscience* 11, 102-107, doi:10.1038/s41561-017-0054-8.

Goodwin, P. (2016) How historic simulation-observation discrepancy affects future warming projections in a very large model ensemble, *Climate Dynamics*, CLDY-D-15-00368R2, doi: 10.1007/s00382-015-2960-z.

Goodwin, P., R.G. Williams and A. Ridgwell (2015), Sensitivity of climate to cumulative carbon emissions due to compensation of ocean heat and carbon uptake, *Nature Geoscience* 8, 29-34. doi:10.1038/ngeo2304.

Goodwin, P., K. I. C. Oliver, and T. M. Lenton (2011), Observational constraints on the causes of Holocene CO2 change, *Global Biogeochemical Cycles*, 25, GB3011, doi:10.1029/2010GB003888.

Goodwin, P., R.G. Williams, A. Ridgwell and M.J. Follows (2009), Climate sensitivity to the carbon cycle modulated by past and future changes in ocean chemistry, *Nature Geoscience*, Vol. 2, No. 2, p145-150, doi:10.1038/ngeo416.

Goodwin, P., M. J. Follows, R. G. Williams (2008), Analytical relationships between atmospheric carbon dioxide, carbon emissions, and ocean processes, *Global Biogeochemical Cycles*, 22, GB3030, doi:10.1029/2008GB003184.

Goodwin, P. and Lenton, T. (2009), Quantifying the feedback between ocean heating and CO2 solubility as an equivalent carbon emission, *Geophysical Research Letters,* 36, L15609, doi:10.1029/2009GL039247.

Goodwin, P., R.G. Williams, M.J. Follows, S. Dutkiewicz (2007), Ocean-atmosphere partitioning of anthropogenic carbon dioxide on centennial timescales, *Global Biogeochemical Cycles*, 21, GB1014, doi:10.1029/2006GB002810.

Gregory, J. M., Ingram, W. J., Palmer, M. A., Jones, G. S., Stott, P. A., Thorpe, R. B., … Williams, K. D. (2004). A new method for diagnosing radiative forcing and climate sensitivity. Geophysical Research Letters, 31, L03205, doi.org/10.1029/2003GL018747

Gregory, J. M., Jones, C. D., Cadule, P. & Friedlingstein, P. (2009) Quantifying carbon cycle feedbacks. *J. Clim*. 22, 5232–5250.

Hansen, J., Ruedy, R., Sato, M. and Lo, K., (2010) Global surface temperature change, *Rev. Geophys.*, 48, RG4004, doi:10.1029/2010RG000345.

IPCC (2013) *Climate Change 2013: The Physical Science Basis* (eds Stocker, T. F. et al.) (Cambridge Univ. Press, Cambridge, 2013).

Ito, T., and Follows, M.J. (2005), Preformed phosphate, soft tissue pump and atmospheric CO2, *J. Mar. Res.*, 63(4), 813– 839, doi:10.1357/0022240054663231.

Knutti, R., Rugenstein, M.A.A. and Hergerl, G.C. (2017) Beyond equilibrium climate sensitivity, *Nature Geoscience* 10, 727-736, DOI:10.1038/ngeo3017.

le Quéré et al. (2018). Global Carbon Budget 2017, *Earth Syst. Sci. Data*, 10, 405-448, doi: 10.5194/essd-10-405-2018.

MacDougall, A. H. and Knutti, R. (2016). Projecting the release of carbon from permafrost soils using a perturbed physics ensemble modelling approach. *Biogeosciences*, 13, 2123–2136, doi: 10.5194/bg-13-2123-2016.

Meinshausen, M. et al. (2011). The RCP greenhouse gas concentrations and theirextensions from 1765 to 2300. *Climatic Change* 109, 213–241.

Myhre, G., et al. (2013) Anthropogenic and Natural Radiative Forcing Supplementary Material. In: *Climate Change 2013: The Physical Science Basis. Contribution of Working Group I to the Fifth Assessment Report of the Intergovernmental Panel on Climate Change* [Stocker, T.F., D. Qin, G.-K. Plattner, M. Tignor, S.K. Allen, J. Boschung, A. Nauels, Y. Xia, V. Bex and P.M. Midgley (eds.)].

Pugh, T. A. M., Jones, C. D., Huntingford, C., Burton, C., Arneth, A., Brovkin, V., et al. (2018). A large committed long-term sink of carbon due to vegetation dynamics. *Earth's Future,* 6. https://doi.org/10.1029/2018EF000935.

Rohling, E. J., Marino, G., Foster, G. L., Goodwin, P. A., von der Heydt, A. S., & Köhler, P. (2018). Comparing climate sensitivity, past and present. *Annual Review of Marine Science*, 10, 261–288. http://www.annualreviews.org/doi/full/10.1146/annurev-marine-121916-063242.

Schwinger, J., Tjiputra, J.F., Heinze, C., Bopp, L., Christian, J.R., Gehlen, M., Ilyina, T., Jones, C.D., Salas-Mélia, D., Segschneider, J. and Séférian, R. (2014) Nonlinearity of ocean carbon cycle feedbacks in CMIP5 earth system models. *Journal of Climate*, *27*(11), pp.3869-3888.

Williams, R.G., Roussenov, V., Goodwin, P., Resplandy, L. and Bopp, L. (2017) Sensitivity of global warming to carbon emissions: effects of heat and carbon uptake in a suite of Earth system models, *Journal of Climate* 30, 9343-9363, doi:10.1175/JCLI-D-16-0468.1

Williams, R. G., P. Goodwin, A. Ridgwell, and P. L. Woodworth (2012), How warming and steric sea level rise relate to cumulative carbon emissions, *Geophys. Res. Lett.*, 39, L19715, doi:10.1029/2012GL052771.

Williams R.G. and Follows, M.J. (2011) *Ocean Dynamics and the Carbon Cycle: Principles and Mechanisms.* Cambridge University Press, ISBN: 9780521843690. 416pp.

Williamson, D., Blaker, A.T., Hampton, C. & Salter, J. (2015). Identifying and removing structural biases in climate models with history matching. *Climate Dynamics* 45, 1299-1324. doi:10.1007/s00382-014-2378-z.

Zickfeld, K., et al. (2013). Long-term climate change commitment and reversibility: An EMIC intercomparison. *Journal of Climate*, 26 (16).

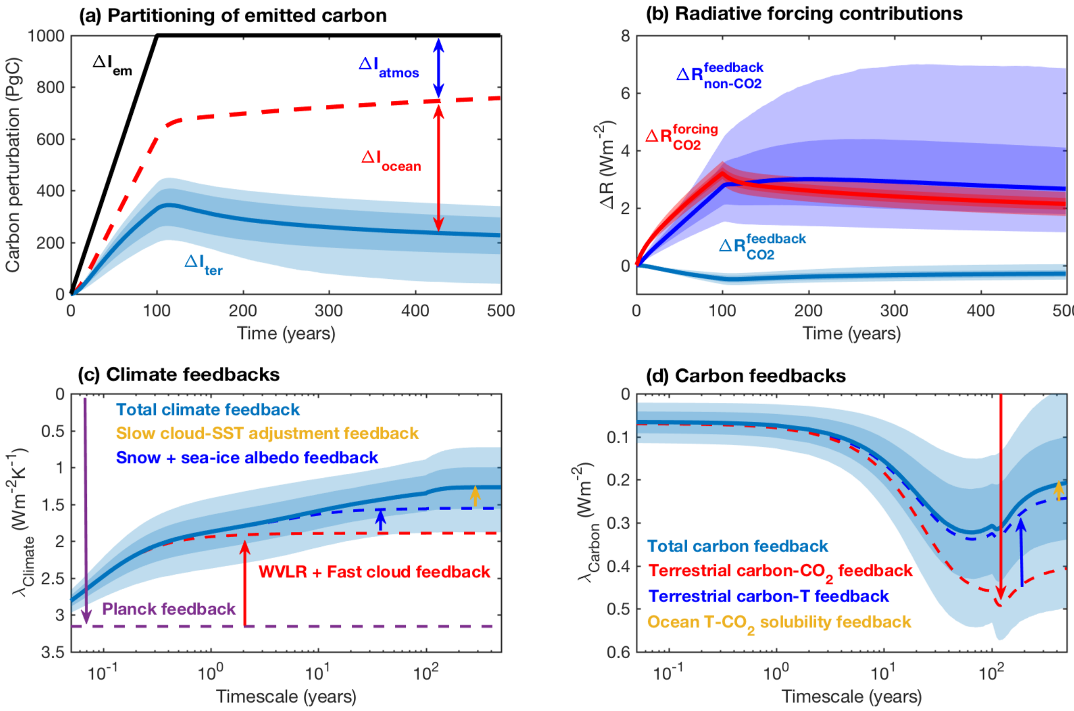

Figure 1: Climate and carbon feedback over time for a 1000PgC emission experiment in a large ensemble of observation-constrained simulations. (a) Partitioning of a 1000PgC carbon emission (ΔI_{em}, black line) between the terrestrial carbon (ΔI_{ter}, light blue line and shading), the ocean (ΔI_{ocean}, red arrow) and the atmospheric inventories (ΔI_{atmos}, bright blue arrow). (b) Radiative forcing contributions from the CO_2 forcing from emissions without carbon feedbacks (red), plus the non-CO_2 feedbacks (blue) and from the carbon feedbacks (light blue). (c) Total climate feedback, λ_{Climate} (light blue line and shading), and (d) total carbon feedback, λ_{Carbon} (light blue line and shading), both showing contributions from individual feedback processes (dashed lines and arrows). On all panels, lines show the ensemble median, dark shading is 66% range and light shading is the 95% range.

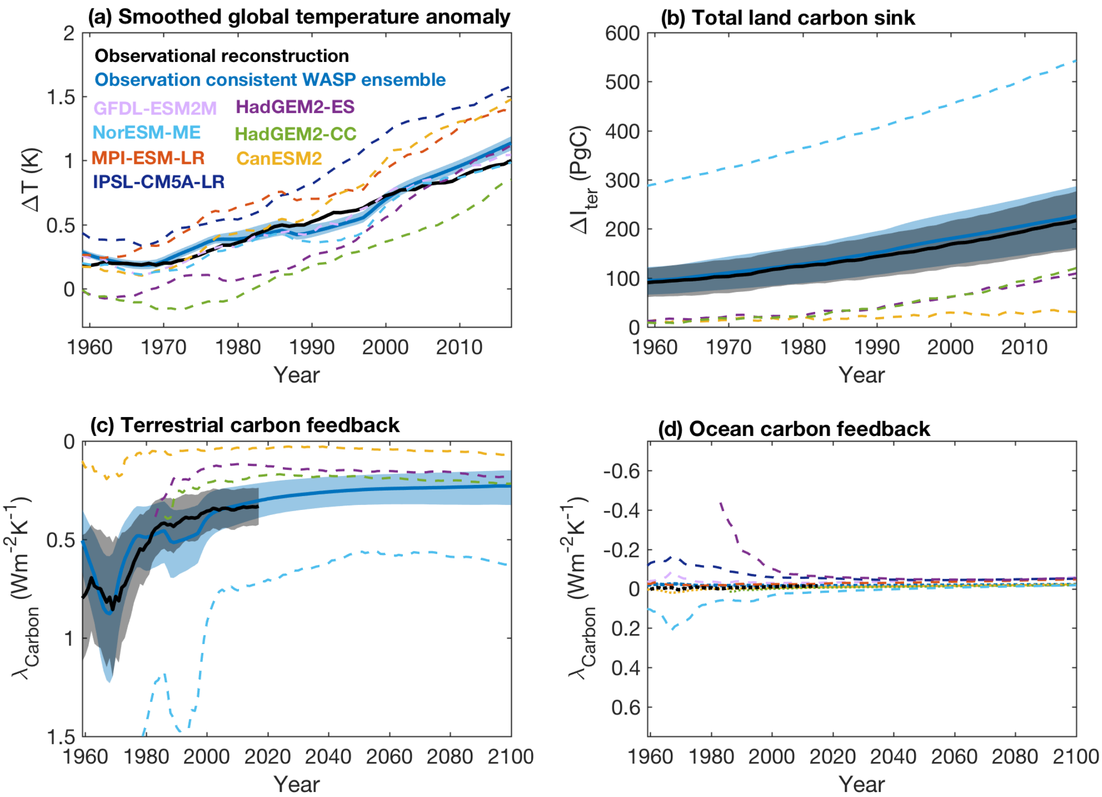

Figure 2: Temperature anomaly, carbon sink and carbon feedback from observational reconstructions (black: shading is $\pm 1\sigma$ range where shown), observation-constrained WASP simulations (blue: line showing median and shading 66% range) and output from 7 CMIP5 Earth system models. (a) 11-year running mean surface temperature anomaly relative to pre-1900 average. Observational reconstructions from GISTEMP. (b) Cumulative terrestrial carbon sink. Observational reconstructions from the Global Carbon Budget (GCB) with additional output from 16 DGVMs to calculate uncertainty. (c) Terrestrial carbon feedback, λ_{Carbon} (eq. 11). Observational reconstructions from GISTEMP and GCB from 1959 to 2017, and simulations using RCP4.5 scenario to project to year 2100. (d) Ocean carbon feedback, λ_{Carbon}, from the CO_2 solubility effect only (dotted lines) and from both ocean biological drawdown and CO_2 solubility effects (dashed lines). Observational reconstructions (black dotted line) derived from *Cheng et al*. (2017) ocean heat uptake combined with GISTEMP.

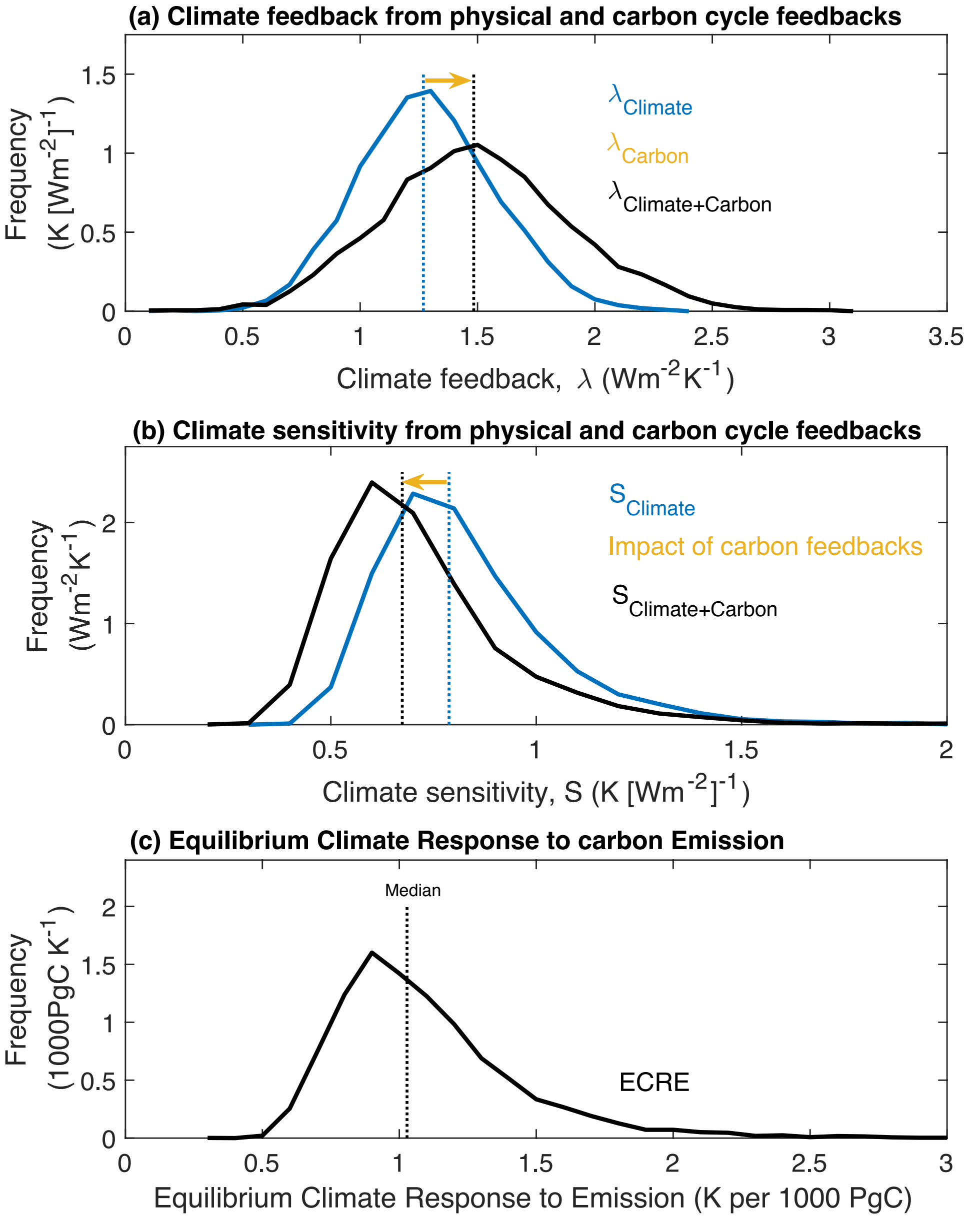

Figure 3: Observational constraints on climate feedback and climate sensitivity from both physical and carbon cycle feedbacks. (a) Climate feedback frequency distributions (solid lines) and median value (dotted lines) for λ_{Climate} (blue) and $\lambda_{\text{Climate+Carbon}} = \lambda_{\text{Climate}} + \lambda_{\text{Carbon}}$ (black). Orange arrow shows the contribution of carbon feedback, λ_{Carbon}, to the median values. (b) Climate sensitivity frequency distributions for S_{Climate} (blue) and $S_{\text{Climate+Carbon}}$ (black), with orange arrow showing impact of carbon feedbacks on the median. (c) Equilibrium Climate Response to carbon Emission (ECRE) frequency distribution (black).